Homogenization of periodic auxetic materials

Justin Dirrenberger, Samuel Forest, Dominique Jeulin, Christophe Colin

Available online at www.sciencedirect.com

ScienceDirect

Procedia Engineering 10 (2011) 1847–1852

Engineering Procedia

ICM11

Homogenization of periodic auxetic materials

J. Dirrenberger[a,*], S. Forest[a], D. Jeulin[a,b], C. Colin[a]

[a]*Centre des Matériaux, MINES-ParisTech, CNRS UMR 7633, BP 87, 91 003 Evry Cedex, France*
[b]*Centre de Morphologie Mathématique, MINES-ParisTech, 35, rue St-Honoré, 77 305 Fontainebleau, France*

Abstract

Materials presenting a negative Poisson's ratio (auxetics) have drawn attention for the past two decades, especially in the field of lightweight composite structures and cellular materials. Studies have shown that auxeticity may result in higher shear modulus, fracture toughness and acoustic damping. In this work, three auxetic periodic lattices are considered. Elastic moduli are computed and anisotropy is investigated by the use of finite element method combined with numerical homogenization technique.

Keywords: Homogenization, Finite element method, Auxetics, Negative Poisson's ratio, Periodic boundary conditions, Architectured materials, Anisotropy, Elasticity

1. Introduction

In the case of isotropic elasticity, mechanical behavior is described by any couple of variables among these: Young's modulus E, Poisson's ratio ν, bulk modulus K and Lamé's coefficients λ and μ (also referred to as G, shear modulus). Poisson's ratio is defined as the ratio of the contraction in the transverse direction to the extension in the longitudinal direction. Thermodynamically, ν lies between -1 and 0.5. Most materials naturally present a positive Poisson's ratio, although negative Poisson's ratio materials, or auxetics [1], have been engineered since the mid-1980s [2–11]. Such materials have been expected to present enhanced mechanical properties such as shear modulus and fracture toughness [12], indentation resistance [13–15] but also acoustic damping [16–18]. Besides, $\nu < 0$ allows synclastic curvature of plates [19], thus enabling the manufacture of doubly-curved sandwich panels without core buckling. Moreover auxetic foams seem to provide better resistance to crash than conventional cellular materials [20].

This paper deals with the numerical determination of the effective elastic tensor components of three auxetic periodic lattices, including a new transversely isotropic microstructure. Finite element method (FEM) coupled with 3D periodic homogenization technique is used to compute elastic moduli and characterize anisotropy. Comparison between the architectured microstructures is made and their use in terms of design and engineering applications is put into perspective.

*Corresponding author
Email address: justin.dirrenberger@mines-paristech.fr (J. Dirrenberger)

1877-7058 © 2011 Publi d by Elsevier Ltd.
doi:10.1016/j.proeng.2011.04.307

2. Numerical homogenization

In this work, numerical homogenization consists in determining effective mechanical properties over a unit-cell (defined by its periodicity vectors $\underline{\boldsymbol{v_i}}$) with periodic boundary conditions (PBC) using FEM [21–23]. Such an approach is quite popular within the mechanics of composites community, while scarce in the auxetics research.

The macroscopic stress and strain tensors $\underset{\sim}{\boldsymbol{\Sigma}}$ and $\underset{\sim}{\boldsymbol{E}}$ are defined by the spatial averages:

$$\underset{\sim}{\boldsymbol{\Sigma}} \hat{=} \langle \underset{\sim}{\boldsymbol{\sigma}} \rangle = \frac{1}{V} \int_V \underset{\sim}{\boldsymbol{\sigma}} \, dV \qquad \underset{\sim}{\boldsymbol{E}} \hat{=} \langle \underset{\sim}{\boldsymbol{\varepsilon}} \rangle = \frac{1}{V} \int_V \underset{\sim}{\boldsymbol{\varepsilon}} \, dV \tag{1}$$

PBC over the unit-cell give displacement field $\underline{\boldsymbol{u}}$ such as:

$$\underline{\boldsymbol{u}} = \underset{\sim}{\boldsymbol{E}}.\underline{\boldsymbol{x}} + \underline{\boldsymbol{v}} \quad \forall \underline{\boldsymbol{x}} \in V \tag{2}$$

with $\underline{\boldsymbol{v}}$ periodic fluctuation. It takes the same value at two homologous points on opposite faces of V, whereas the traction vector $\underline{\boldsymbol{t}} = \underset{\sim}{\boldsymbol{\sigma}}.\underline{\boldsymbol{n}}$ takes opposite values, $\underline{\boldsymbol{n}}$ being the normal vector. By applying either macroscopic strain or stress, one can compute the effective elastic moduli fourth-rank tensor $\underset{\approx}{\boldsymbol{C}}$ and compliance tensor $\underset{\approx}{\boldsymbol{S}}$ of materials:

$$\underset{\sim}{\boldsymbol{\Sigma}} = \underset{\approx}{\boldsymbol{C}} : \underset{\sim}{\boldsymbol{E}} \qquad \underset{\sim}{\boldsymbol{E}} = \underset{\approx}{\boldsymbol{S}} : \underset{\sim}{\boldsymbol{\Sigma}} \tag{3}$$

3. Sandwich core microstructures

3.1. Hexachiral lattice

This chiral microstructure was first proposed by Lakes in 1991 [6], then fabricated and studied by Prall and Lakes in 1997 [9] and Alderson *et al.* in 2009 [11]. Based on the the parameters defined in [11], cell geometry can be described this way: the circular nodes have radius r, the ligaments have length L, and both have in common wall thickness t (cf. Figure 1(a)) as well as depth d, which in our case is considered infinite due to periodicity conditions. Hence, three dimensionless parameters are defined: $\alpha = \mathrm{L/r}$, $\beta = \mathrm{t/r}$ and $\gamma = \mathrm{d/r}$. On Figure 1(b), $\alpha = 5, \beta = 0.1$ and $\gamma \to +\infty$. These parameters correspond to a volume fraction of 7%. The 6–fold symmetry provides transverse isotropy.

3.2. Tetra-antichiral lattice

This microstructure was proposed and studied by Alderson *et al.* in 2009 [11]. Cell geometry can be described exactly as for the hexachiral lattice (cf. Figure 2(a)). Here, $\alpha = 10, \beta = 0.25$ and $\gamma \to +\infty$ (cf. Figure 2(b)). Volume fraction is 6%. The cell presents 3 orthogonal planes of symmetry, which corresponds to orthotropic elasticity.

3.3. Rotachiral lattice

This chiral microstructure has been designed for this work based on ideas from [10] and [9], the aim was to study the impact of ligaments geometry on auxeticity for chiral lattices. Cell geometry is similar to the hexachiral case, except for the straight ligaments that have been replaced by circular ones with diameter D (cf. Figure 3(a)). Another dimensionless parameter is defined: $\delta = \mathrm{D/r}$. As shown on Figure 3(b), $\delta = 2, \beta = 0.1$ and $\gamma \to +\infty$. Volume fraction is 7%. The 6–fold symmetry provides transverse isotropy.

4. Numerical results

Elastic moduli are computed for a comparable volume fraction ($V_V \sim 0.06$–0.07) using Z-Set FEM software[1] (Figures 5, 4.2 and 4.3). An isotropic bulk material with Young's modulus $E_0 = 210000$ MPa and Poisson's ratio $\nu_0 = 0.3$ is considered. Components are expressed in MPa using Voigt notation. ν^{eff} is the effective Poisson's ratio, $E = \frac{E^{\mathrm{eff}}}{E_0 \times V_V}$ characterizes the elastic modulus along the traction vector $\underline{\boldsymbol{l}}$. $\mu = \frac{\mu^{\mathrm{eff}}}{\mu_0 \times V_V}$ is the normalized shear modulus, with $\mu_0 = \frac{E_0}{2(1+\nu_0)}$. Angles θ and ϕ are used to describe the anisotropy, as shown on Figure 4. In-plane elastic properties (functions of θ) are studied for all lattices (Table 1 and Figure 8(d)), although their use in engineering applications might involve out-of-plane loading. Hence, ν^{eff}, E and μ were also plotted against ϕ (Figures 8(a), 8(b) and 8(c)).

[1] http://www.nwnumerics.com/

(a) Hexachiral unit-cell (b) Hexachiral lattice

Figure 1: Periodic cell with geometric parameters (left). Hexachiral lattice with unit-cell (blue) and periodicity vectors $\underline{\boldsymbol{v_1}}$ and $\underline{\boldsymbol{v_2}}$ (red).

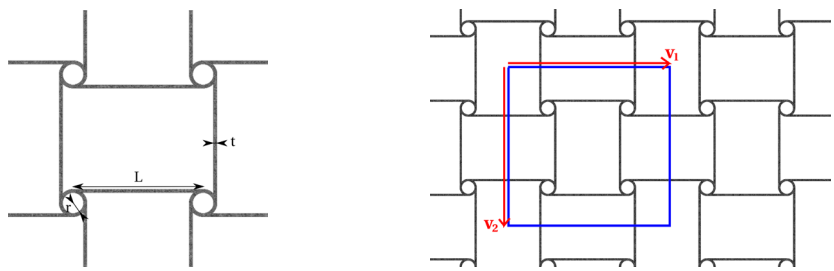

(a) Tetra-antichiral unit-cell (b) Tetra-antichiral lattice

Figure 2: Periodic cell with geometric parameters (left). Tetra-antichiral lattice with unit-cell (blue) and periodicity vectors $\underline{\boldsymbol{v_1}}$ and $\underline{\boldsymbol{v_2}}$ (red).

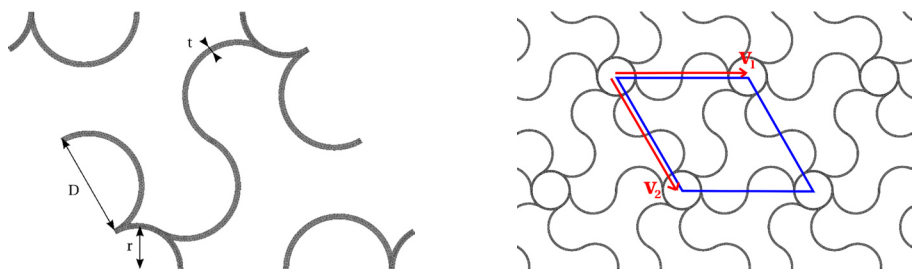

(a) Rotachiral unit-cell (b) Rotachiral lattice

Figure 3: Periodic cell with geometric parameters (left). Rotachiral lattice with unit-cell (blue) and periodicity vectors $\underline{\boldsymbol{v_1}}$ and $\underline{\boldsymbol{v_2}}$ (red).

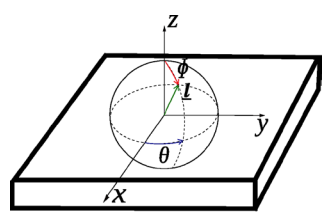

Figure 4: Definition of angles θ and ϕ with respect to the plate.

4.1. Hexachiral lattice

Transverse isotropy is verified since $\frac{C_{11}-C_{12}}{2} = C_{66}$. Components were used to obtain the in-plane properties gathered in Table 1. ν^{eff} is similar to the value from [11], while our estimation of the normalized Young's modulus E is higher. This is discussed later. Figure 8(a) shows an increase of E when the material is streched out-of-plane. Poisson's ratio ν^{eff} is always negative, except for $\phi = 0$ and $\phi = \pi$ where it takes the bulk material value 0.3.

Normalized shear modulus μ can be either higher or lower than in-plane value depending on angle ϕ.

$$[\underset{\approx}{\boldsymbol{C}}] = \begin{bmatrix} 231 & -193 & 114 & 0 & 0 & 0 \\ -193 & 231 & 114 & 0 & 0 & 0 \\ 114 & 114 & 15731 & 0 & 0 & 0 \\ 0 & 0 & 0 & 2271 & 0 & 0 \\ 0 & 0 & 0 & 0 & 2271 & 0 \\ 0 & 0 & 0 & 0 & 0 & 212 \end{bmatrix}$$

Figure 5: Effective elastic moduli tensor for the hexachiral lattice

4.2. Tetra-antichiral lattice

While its geometry is orthotropic, the tensor given below indicates quadratic elasticity (invariant by rotation of $\frac{\pi}{2}$ in the plane). The small dissymmetry is negligible at the scale of the homogenized material. Figure 8(d) shows that in the cell's principal directions, ν^{eff} is similar to the value from [11], but the normalized Young's modulus E is higher. Besides, μ fluctuates over 4 decades and reaches its minimum in the ν^{eff} is close to -1. ν^{eff} is negative for short angle intervals. E is varying over one order of magnitude depending on θ. Figure 8(c) is very comparable with Figure 8(a) in terms of values and angles. E is higher than or equal to in-plane values. ν^{eff} is always negative, except for $\phi = 0$ and $\phi = \pi$ where it takes the bulk material value $\nu^{\text{eff}} = 0.3$. μ fluctuates more with θ than with ϕ.

$$[\underset{\approx}{\boldsymbol{C}}] = \begin{bmatrix} 1365 & -1329 & 10.9 & 0 & 0 & 0 \\ -1329 & 1365 & 10.9 & 0 & 0 & 0 \\ 10.9 & 10.9 & 12613 & 0 & 0 & 0 \\ 0 & 0 & 0 & 1978 & 0 & 0 \\ 0 & 0 & 0 & 0 & 1978 & 0 \\ 0 & 0 & 0 & 0 & 0 & 2.01 \end{bmatrix}$$

Figure 6: Effective elastic moduli tensor for the tetra-antichiral lattice

4.3. Rotachiral lattice

Elastic moduli fourth-rank tensor components for the rotachiral lattice are given below. As for the hexachiral lattice, transverse isotropy is verified by the following relationship $\frac{C_{11}-C_{12}}{2} = C_{66}$. The in-plane moduli and Poisson's ratio are listed in Table 1. Normalized elastic moduli E and μ are about one order of magnitude lower than for the hexachiral lattice. Figure 8(b) shows an increase of E when the material is streched out-of-plane. Poisson's ratio ν^{eff} is always negative, except for $\phi = 0$ and $\phi = \pi$ where it takes the bulk material value 0.3. Normalized shear modulus μ is always higher than its in-plane counterpart.

$$[\underset{\approx}{\boldsymbol{C}}] = \begin{bmatrix} 11 & -2.45 & 2.56 & 0 & 0 & 0 \\ -2.45 & 11 & 2.56 & 0 & 0 & 0 \\ 2.56 & 2.56 & 16173 & 0 & 0 & 0 \\ 0 & 0 & 0 & 1757 & 0 & 0 \\ 0 & 0 & 0 & 0 & 1757 & 0 \\ 0 & 0 & 0 & 0 & 0 & 6.72 \end{bmatrix}$$

Figure 7: Effective elastic moduli tensor for the rotachiral lattice

5. Discussion

Values obtained in this work for E (Table 1) exceed those from [11]. This is due to the boundary conditions of the FEM problem. With periodicity over displacements and nodal force loading, the loading in [11] correponds to a static uniform boundary conditions (SUBC) micromechanical problem, which is known for underestimating elastic moduli

	Hexachiral	Rotachiral
ν^{eff}	-0.83	-0.25
E	4.45×10^{-3}	6.46×10^{-4}
μ	3.50×10^{-2}	1.08×10^{-3}

Table 1: In-plane Poisson's ration and normalized elastic moduli for hexachiral and rotachiral lattices

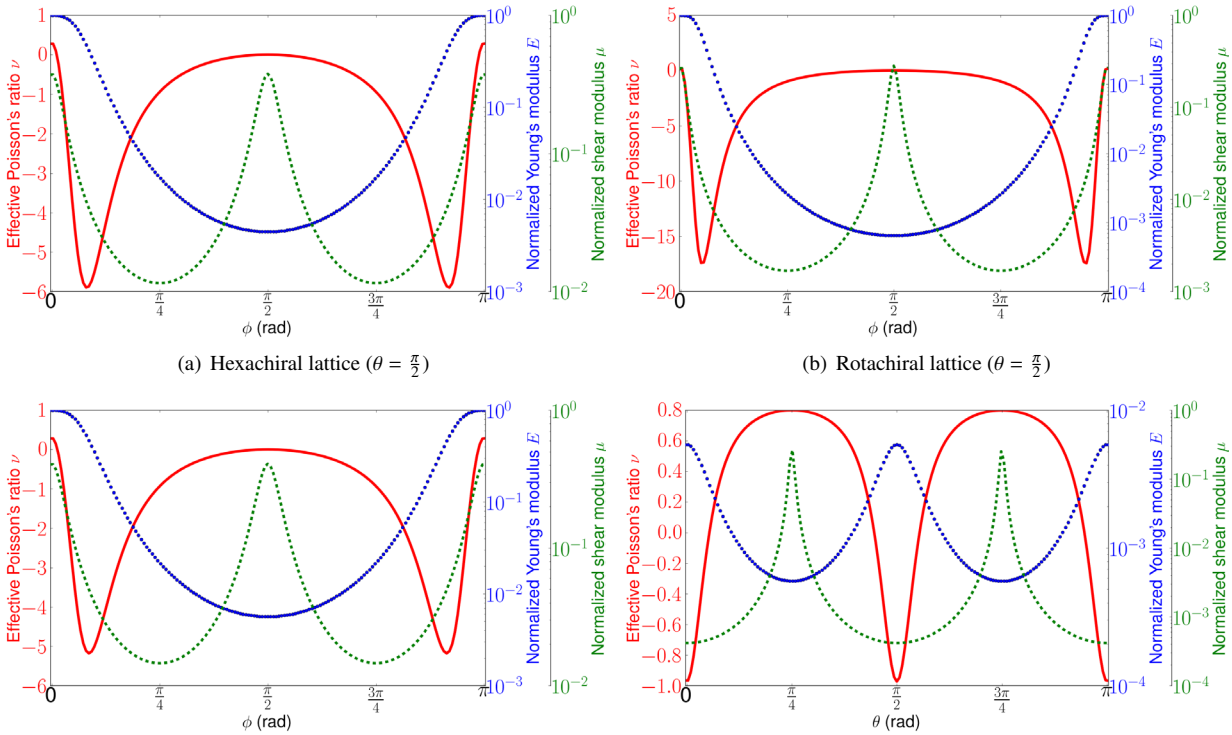

(a) Hexachiral lattice ($\theta = \frac{\pi}{2}$)

(b) Rotachiral lattice ($\theta = \frac{\pi}{2}$)

(c) Tetra-antichiral lattice ($\theta = \frac{\pi}{2}$)

(d) Tetra-antichiral lattice ($\phi = \frac{\pi}{2}$)

Figure 8: ν^{eff} (solid line, red), E (dotted line, blue) and μ (dashed line, green) as functions of angles ϕ and θ

[21]. On the other hand, the PBC problem gives exact results for an infinite medium. The hexachiral, rotachiral and tetra-antichiral lattices all present a strong anisotropy when loaded out-of-plane (cf. Figures 8(a), 8(b) and 8(c)). Extreme Poisson's ratio value of -17 can be reached for the rotachiral lattice (Figure 8(b)). It is worth noting that the tetra-antichiral lattice presents a negative in-plane Poisson's ratio only for quite small angle intervals. Interestingly, ν^{eff} is always negative when a function of angle ϕ. The hexachiral and tetra-antichiral lattices show comparable values in terms of magnitude for normalized elastic moduli as functions of ϕ. For the same volume fraction, the impact on mechanical properties from the change in ligaments geometry between hexachiral and rotachiral lattices is critical: circular ligaments give values which are one order of magnitude lower for both E and μ.

6. Conclusions and prospects

Elastic moduli of three periodic auxetic lattices have been computed using numerical homogenization technique coupled with FEM. The hexachiral is found to present high in-plane elastic moduli and Poisson's ratio close to -1. With its circular (or elliptic) ligaments, the auxetic rotachiral lattice provides a parameter for tuning the microstructure [24] for specific absorption properties. This lattice can exhibit highly negative Poisson's ratio when loaded out-of-plane. The orthotropy of the tetra-antichiral lattice was investigated numerically, showing higher stiffness E in the principal directions of the cell. For this microstructure, auxetic effects in the plane are restricted to short angle intervals around

the principal directions. Such lattices can be used in replacement of traditional honeycomb-core for sandwich panels, especially if produced by extrusion. Samples were made using selective laser melting, a powder metallurgy process, extending one's microstructural design spectrum from 2D to 3D. This method has already been used successfully by others for auxetics [25, 26]. New tridimensional auxetic quasi-isotropic microstructures could be developed using this technique in the near future. Numerical results will be confronted to experimental data currently being obtained. The influence of auxeticity on plasticity has to be evaluated. For industrial applications, non-linear phenomena such as buckling have to be taken into account.

Acknowledgments

This work is part of the MANSART (Architectured sandwich materials) project ANR-08-MAPR-0026. Financial support of ANR is gratefully acknowledged.

References

[1] K. E. Evans, M. A. Nkansah, I. J. Hutchinson, S. C. Rogers, Molecular network design, Nature 353 (1991) 124.
[2] R. F. Almgren, An isotropic three-dimensional structure with Poisson's ratio=-1, Journal of Elasticity 15 (1985) 427–430.
[3] R. S. Lakes, Foam Structures with a Negative Poisson's Ratio, Science 235 (1987) 1038–1040.
[4] R. J. Bathurst, L. Rothenburg, Note on a random isotropic granular material with negative Poisson's ratio, International Journal of Engineering Science 26 (4) (1988) 373–383.
[5] B. D. Caddock, K. E. Evans, Microporous materials with negative Poisson's ratios: I. Microstructure and mechanical properties, Journal of Physics D: Applied Physics 22 (1989) 1877–1882.
[6] R. S. Lakes, Deformation mechanisms in negative Poisson's ratio materials: structural aspects, Journal of Materials Science 26 (1991) 2287–2292.
[7] L. Rothenburg, A. A. Berlin, R. J. Bathurst, Microstructure of isotropic materials with negative Poisson's ratio, Nature 354 (1991) 470–472.
[8] G. W. Milton, Composite Materials with Poisson's Ratios Close to -1, Journal of the Mechanics and Physics of Solids 40 (5) (1992) 1105–1137.
[9] D. Prall, R. S. Lakes, Properties of a Chiral Honeycomb with a Poisson's Ratio of -1, International Journal of Mechanical Sciences 39 (3) (1997) 305–314.
[10] N. Gaspar, X. J. Ren, C. W. Smith, J. N. Grima, K. E. Evans, Novel honeycombs with auxetic behaviour, Acta Materialia 53 (2005) 2439–2445.
[11] A. Alderson, K. L. Alderson, D. Attard, K. E. Evans, R. Gatt, J. N. Grima, W. Miller, N. Ravirala, C. W. Smith, K. Zied, Elastic constants of 3-, 4- and 6-connected chiral and anti-chiral honeycombs subject to uniaxial in-plane loading, Composites Science and Technology 70 (7) (2010) 1042–1048.
[12] J. B. Choi, R. S. Lakes, Fracture toughness of re-entrant foam materials with a negative Poisson's ratio: experiment and analysis, International Journal of Fracture 80 (1996) 73–83.
[13] R. S. Lakes, Materials with structural hierarchy, Nature 361 (1993) 511–515.
[14] K. L. Alderson, A. P. Pickles, P. J. Neale, K. E. Evans, Auxetic Polyethylene - The Effect of a Negative Poisson Ratio on Hardness, Acta Metallurgica et Materialia 42 (7) (1994) 2261–2266.
[15] K. L. Alderson, A. Fitzgerald, K. E. Evans, The strain dependent indentation resilience of auxetic microporous polyethylene, Journal of Materials Science 35 (16) (2000) 4039–4047.
[16] A. W. Lipsett, A. I. Beltzer, Reexamination of Dynamic Problems of Elasticity for Negative Poisson's Ratio, Journal of the Acoustical Society of America 84 (6) (1988) 2179–2180.
[17] C. P. Chen, R. S. Lakes, Micromechanical analysis of dynamic behavior of conventional and negative Poisson's ratio foams, Journal of Engineering Materials and Technology 118 (3) (1996) 285–288.
[18] I. Chekkal, M. Bianchi, C. Remillat, F.-X. Becot, L. Jaouen, F. Scarpa, Vibro-acoustic properties of auxetic open cell foam: Model and experimental results, Acta Acustica united with Acustica 96 (2) (2010) 266–274.
[19] K. E. Evans, The design of doubly curved sandwich panels with honeycomb cores, Composite Structures 17 (2) (1991) 95–111.
[20] F. Scarpa, J. R. Yates, L. G. Ciffo, S. Patsias, Dynamic crushing of auxetic open-cell polyurethane foam, Proceedings of the Institution of Mechanical Engineers Part C-Journal of Mechanical Engineering Science 216 (12) (2002) 1153–1156.
[21] T. Kanit, S. Forest, I. Galliet, V. Mounoury, D. Jeulin, Determination of the size of the representative volume element for random composites: Statistical and numerical approach, International Journal of Solids and Structures 40 (2003) 3647–3679.
[22] K. Madi, S. Forest, P. Cordier, M. Boussuge, Numerical study of creep in two-phase aggregates with a large rheology contrast: implications for the lower mantle, Earth and Planetary Science Letters 237 (1-2) (2005) 223–238. doi:10.1016/j.epsl.2005.06.027.
[23] A. Jean, G. C. Engelmayr, Finite element analysis of an accordion-like honeycomb scaffold for cardiac tissue engineering, Journal of Biomechanics 43 (2010) 3035–3043.
[24] M. F. Ashby, Y. Bréchet, Designing hybrid materials, Acta Materialia 51 (2003) 5801–5821.
[25] X. Huang, S. Blackburn, Developing a New Processing Route to Manufacture Honeycomb Ceramics with Negative Poisson's Ratio, Key Engineering Materials 206-213 (2002) 201–204.
[26] J. Schwerdtfeger, P. Heinl, R. F. Singer, C. Körner, Auxetic cellular structures through selective electron-beam melting, Physica Status Solidi (b) 247 (2) (2010) 269–272.